This is the accepted manuscript made available via CHORUS. The article has been published as:

Magneto-optical response of the magnetic semiconductors math xmlns="http://www.w3.org/1998/Math/MathML">mrow>msub>mrow>mi>EuCd/mi>/mrow>mn>2/mn>/msub>msub>mi>X/mi>mn>2/mn>/msub>/mrow>/math> (math xmlns="http://www.w3.org/1998/Math/MathML">mi>X/mi>/math>=P, As, Sb)

S. Nasrallah, D. Santos-Cottin, F. Le Mardelé, I. Mohelský, J. Wyzula, L. Akšamović, P. Sačer, J. W. H. Barrett, W. Galloway, K. Rigaux, F. Guo, M. Puppin, I. Živković, J. H. Dil, M. Novak, C. C. Homes, M. Orlita, N. Barišić, and Ana Akrap

Phys. Rev. B **110**, L201201 — Published 18 November 2024

DOI: 10.1103/PhysRevB.110.L201201

Magneto-optical response of magnetic semiconductors $EuCd_2X_2$ (X= P, As, Sb)

S. Nasrallah,[1,2,*] D. Santos-Cottin,[1] F. Le Mardelé,[3] I. Mohelský,[3] J. Wyzula,[1] L. Akšamović,[2] P. Sačer,[4] J. W. H. Barrett,[1,5] W. Galloway,[1,5] K. Rigaux,[6] F. Guo,[6] M. Puppin,[6] I. Živković,[7] J.H. Dil,[6] M. Novak,[4] C. C. Homes,[8] M. Orlita,[3,9] N. Barišić,[2,4,†] and Ana Akrap[1,4,‡]

[1] *Department of Physics, University of Fribourg, 1700 Fribourg, Switzerland*
[2] *Institute of Solid State Physics, TU Wien, A-1040 Vienna, Austria*
[3] *LNCMI; CNRS-UGA-UPS-INSA; 25, avenue des Martyrs, F-38042 Grenoble, France*
[4] *Department of Physics, Faculty of Science, University of Zagreb, Bijenička 32, HR-10000 Zagreb, Croatia*
[5] *University of Cambridge, UK*
[6] *Lausanne Centre for Ultrafast Science (LACUS), École Polytechnique Fédérale de Lausanne (EPFL), CH-1015 Lausanne, Switzerland*
[7] *Institut de Physique, École Polytechnique Fédérale de Lausanne (EPFL), CH-1015 Lausanne, Switzerland*
[8] *National Synchrotron Light Source II, Brookhaven National Laboratory, Upton, New York 11973, USA*
[9] *Institute of Physics, Charles University, CZ-12116 Prague, Czech Republic*

(Dated: October 22, 2024)

In this study, we identify $EuCd_2X_2$ (for X = P, As, Sb) as a series of magnetic semiconductors. We examine how the band gap of the series responds to X changing from phosphorus (P), to arsenic (As), and finally antimony (Sb). We characterize the samples using electronic transport and magnetization measurements. Based on infrared spectroscopy, we find that the band gap reduces progressively from 1.23 eV in $EuCd_2P_2$, to 0.77 eV in $EuCd_2As_2$, and finally 0.52 eV in $EuCd_2Sb_2$. In a magnetic field, all three systems show a strong response and their band gaps decrease at 4 K. This decrease is non-monotonic as we change X. It is strongest in the phosphorous compound and weakest in the antimony compound. For all the three compositions, $EuCd_2X_2$ remains a semiconductor up to the highest magnetic field applied (16 T).

Recent work in infrared optics and magneto-optics has unveiled that $EuCd_2As_2$ is a magnetic semiconductor, with a band gap of 770 meV [1–5]. In a magnetic field, the energy gap is strongly reduced, but the system remains gapped even in high magnetic fields. This finding challenged the previously assumed topological semimetal nature of $EuCd_2As_2$, where electronic transport measurements indicated a metal-like behavior at elevated temperatures [4], *ab initio* calculations indicated the Weyl points [6–8], and angle-resolved photoemission spectroscopy (ARPES) measurements revealed a conical shape of the valence band [9].

Several recent studies reproduced $EuCd_2As_2$ samples with activated resistivity behavior [2–4], and confirmed the presence of a significant band gap in $EuCd_2As_2$. The question remains: How does chemically tuning the system's composition affect the ground state?

In the present study, we substituted As with Sb and P to investigate if these sister compounds exhibit similar behavior. We employed infrared and magneto-infrared spectroscopy, complemented with measurements of transport and magnetic properties, to probe the band structure. Our main finding is that the band gap progresses from 1.23 eV in $EuCd_2P_2$, to 0.77 eV in $EuCd_2As_2$, and finally 0.52 eV in $EuCd_2Sb_2$ at low temperature. In a magnetic field, all three systems exhibit a strong magneto-optical response, leading to a reduction in their respective band gaps. This is most prominent in the phosphorus compound, where the band gap is diminished by 150 meV in a field of 0.8 T. Conversely, the smallest decrease is observed in the antimony compound, where 2 T reduced the band gap by 45 meV. Despite these variations, all three compositions remain semiconducting even under high magnetic fields.

Single crystals of high purity $EuCd_2X_2$ were synthesized using the Sn flux method [1]. The synthesis process involved a two-step approach, utilizing crystals from the initial growth as seeds. The trigonal crystal structure of $EuCd_2X_2$ is shown in Fig. 1(a), where the Cd and X layers are situated between the Eu layers [10, 11]. For material characterization, a Physical Properties Measurement System was used to measure resistance up to 300 K. Additionally, characterization included the use of a Superconducting Quantum Interference Device to measure magnetic susceptibility up to 100 K at 10 Oe and 100 Oe, as well as magnetization in a magnetic field up to 7 T at 4 K. Angle-resolved photoelectron spectroscopy (ARPES) experiment was carried out at the EPFL LACUS, at the ASTRA end station. The ARPES measurement was carried out at 80 K using a photon energy of 36.8 eV. Single crystals were cleaved *in situ* at a base pressure better than 1×10^{-10} mbar. Given the absence of states at the Fermi level in $EuCd_2P_2$, polycrystalline Cu was used as a reference for the binding energy. Infrared reflectance was measured using a Vertex 70v optical spectrometer, while infrared transmission and magneto-transmission measurements were performed using a Vertex 80v optical spectrometer.

* serena.nasrallah@tuwien.ac.at
† neven.barisic@tuwien.ac.at
‡ aakrap.phy@pmf.hr

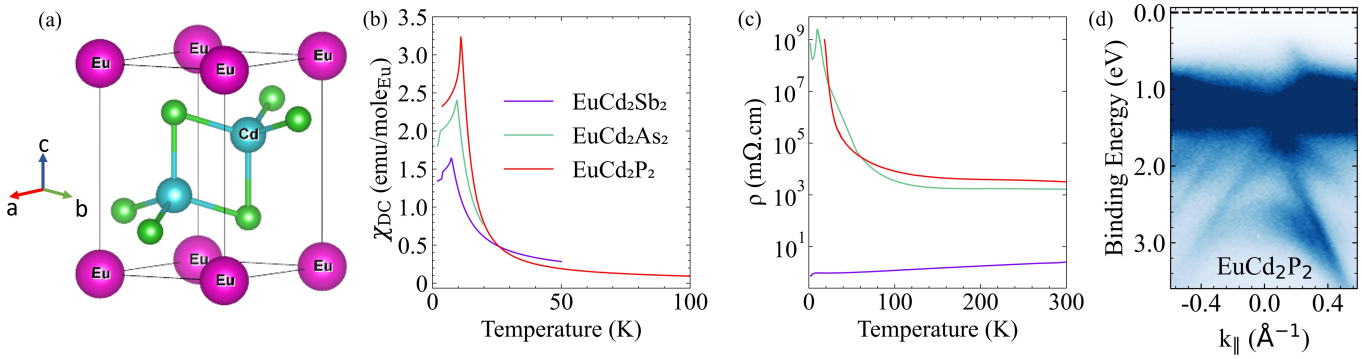


Figure 1. (a) The primitive unit cell of $EuCd_2X_2$ (X = Sb, As, P) shows a trigonal crystal structure. (b) The magnetic susceptibility while the magnetic field is parallel to the c-axis as a function of temperature measured at 10 Oe for Sb and P and at 100 Oe for As; the pronounced peak indicates the Néel temperature (T_N) values of 7.3 K, 9.5 K, and 11 K, respectively, for X = Sb, As, and P. (c) The resistivity as a function of temperature for $EuCd_2X_2$ (X = Sb, As, P). (d) Static ARPES band map of $EuCd_2P_2$ along the $\overline{M}$-$\overline{\Gamma}$-$\overline{M}$ symmetry point.

Peaks in the magnetic susceptibility χ_{DC} = M/H (Fig. 1(b)) at T_N = 11 K [12], 9.5 K [11], and 7.3 K [10, 13] for $EuCd_2X_2$ (X = P, As, and Sb), correspond to the antiferromagnetic ordering transition. Around 4 K, a sharp drop in susceptibility indicates the presence of Sn flux on sample surface, as reported in [1]. However, the Sn flux does not affect the sample quality [14]. Although the χ_{DC} shows similar behaviour for different X, their electrical resistivity are quite different. $EuCd_2Sb_2$ exhibits a modest metallic behavior at high temperatures [10] with a resistivity of 2.5 mΩcm at 300 K. We may conclude that the Fermi energy (E_F) is located within the valence band. In contrast, $EuCd_2As_2$ displays activated behavior with an activation energy of 26 meV and a high resistivity of 2.5×10^9 mΩcm at 10 K. The resistivity of $EuCd_2P_2$ reaches 9.9×10^8 mΩcm at 20 K with an activation energy of 16 meV. At lower temperatures the resistivity becomes inaccessible for our measurement. We may conclude that in $EuCd_2As_2$ and $EuCd_2P_2$ the Fermi energy is within the band gap. The location of E_F is governed by impurity and defect chemistry material synthesis.

While we were unable to measure the resistive peak in the phosphorus compound, in both arsenide and antimonide the resistive peaks coincide with the antiferromagnetic ordering peaks in the magnetic susceptibility. The increase in resistance near T_N is still not fully understood. One possibility is that above T_N, $EuCd_2As_2$ and $EuCd_2Sb_2$ exhibit enhanced scattering due to magnetic fluctuations [15]. This effect is more pronounced in As than in Sb, resulting in a stronger peak in As. There is also a suggestion that in $EuCd_2P_2$ ferromagnetic clusters are formed above T_N as a result of the spins of charge carriers interacting with the magnetic moments of Eu. These clusters then localize the carriers, leading to an increasing resistance [12, 16]. To confirm the correct band structure of $EuCd_2P_2$, photoemisssion measurement were performed. Figure 1(d) shows a static ARPES band map of $EuCd_2P_2$ at 80 K along the $\overline{M}$-$\overline{\Gamma}$-$\overline{M}$ symmetry point. ARPES data show the presence of Eu $4f$ states as broad features centered around 1-1.2 eV binding energy. At the Γ point, there are several hole-like bands, which according to Usachov et al. originate mainly from the p-orbits of phosphorus [16]. ARPES data on $EuCd_2As_2$ show a similar band map, with $4f$ centered around 1.5 eV [1].

All the three compounds belong to the $P\bar{3}m1$ space group, so they have four Raman-active phonons and four IR-active phonons within the irreducible vibrational representation, $\Gamma_{irr} = 2A_{1g} + 2E_g + 2A_{2u} + 2E_u$ [17]. The A_{1g} and E_g modes are Raman active, while the A_{2u} and E_u modes are infrared active along the c-axis and within the ab planes, respectively [17]. The low-energy infrared reflectance measured at 10 K for light polarized in the ab planes is shown in Fig. 2(a). The response is different upon changing from Sb to P in the $EuCd_2X_2$. In the far-infrared (FIR) range, phonons in $EuCd_2Sb_2$ are screened by itinerant carriers, consistent with a metallic resistivity. On the contrary, for $EuCd_2As_2$, the reflectance is dominated by two strong in-plane E_u phonon modes at 86 and 165 cm^{-1} [1]. The two phonon modes remain unscreened because free carriers are nearly absent. In the case of $EuCd_2P_2$, similar behavior is observed with two E_u phonon modes at approximately 89 and 241 cm^{-1} [17]. Notably, there is a larger longitudinal optical mode and transversal optical mode (LO-TO) splitting in $EuCd_2P_2$ than that in $EuCd_2As_2$.

In the As and P compounds, the low-frequency phonons are observed at nearby frequencies: 86 cm^{-1} for As, and 89 cm^{-1} for P. The lower in energy E_u phonon mode of Sb, highly screened by free charge carriers, was not observed at the level of the signal-to-noise ratio of our data. However, it is expected to occur at frequencies lower than those of As and P, but still in close proximity. The low-frequency E_u mode is caused by in-plane atomic displacements that predominantly involve out-of-phase movements between the Eu and Cd atoms, with minimal contribution from the X atoms, which align in phase with the Cd atoms [17]. Our data confirms that

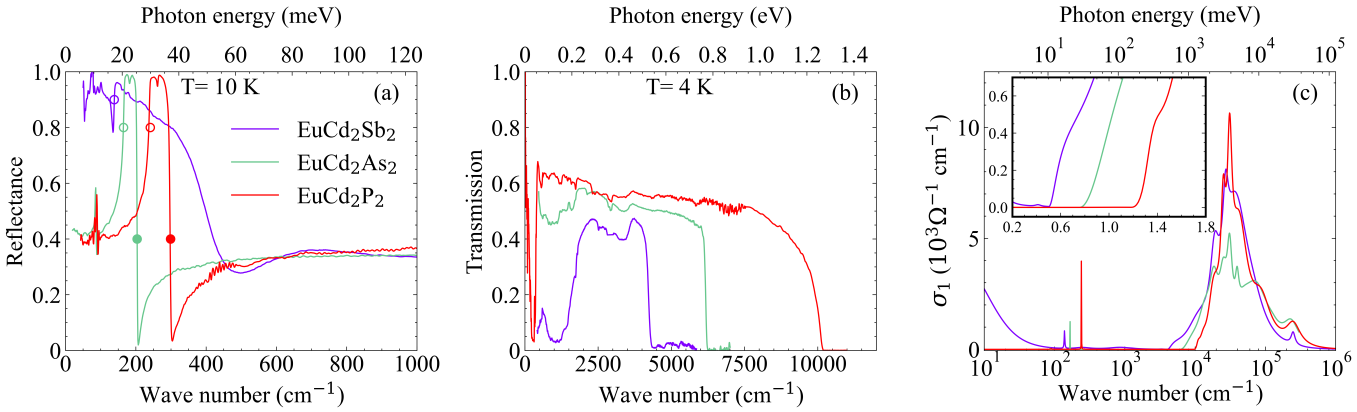


Figure 2. (a) Low energy reflectance of $EuCd_2X_2$ (X = Sb, As, P) at 10 K . The empty circle indicates the phonon TO modes and the filled one indicates the phonon LO modes. (b) Energy transmission at 4 K exhibits an energy gap of 0.52 eV, 0.77 eV, and 1.23 eV, respectively, for $EuCd_2X_2$ (X = Sb, As, P). (c) Multi-layer modeling of the real part of the optical conductivity, $\sigma_1(\omega)$, in the whole energy range. The inset illustrates the optical conductivity in the absorption onset region as a function of wave number.

the X atoms do not significantly affect this oscillation, as indicated by the close frequencies observed in the different compounds. We next focus on the second E_u mode that is well observed in all three compounds, with its TO mode indicated by an empty circle and its LO mode by a full circle in Fig. 2(a). The LO mode is not visible in the Sb compound, because of strong screening. A noticeable change occurs when transitioning from $EuCd_2Sb_2$ to $EuCd_2P_2$: the energy of the second phonon shifts to a higher value while getting broader. The TO mode of the second phonon for the three compounds is at rather different frequencies, unlike the low energy phonon. This significant difference is attributed to the nature of this second E_u mode, which mainly involves the out-of-phase displacement of the Sb, As, and P atoms relative to the Cd and Eu atoms. The observed dependence of the phonon energy on the crystal composition correlates well with the atomic masses of Sb, As and P [18].

More information can be obtained from the reflectivity data, such as ϵ_e, which is the dielectric constant coming from the interband electronic excitations (sometimes referred to as ϵ_∞). After the second resonance, the reflectivity is approximately flat, with $R_{\infty,Sb} = 0.42$, $R_{\infty,As} = 0.37$, and $R_{\infty,P} = 0.4$. R_∞ is related to ϵ_e, and a flat reflectivity implies that the dielectric function and the refractive index are real [19], so we can obtain ϵ_e from

$$R = \left|\frac{\sqrt{\epsilon}-1}{\sqrt{\epsilon}+1}\right|^2 \tag{1}$$

Since all three samples are transparent in the mid-infrared (MIR) and near-infrared (NIR), as shown in Fig. 2(b), the reflectivity is overestimated in those regions, and therefore ϵ_e is overestimated. To solve this issue and extract different optical response functions, like the dielectric function or optical conductivity, one can model transmission and reflectance using a multi-layer dielectric response [20]. The real part of the optical conductivity, $\sigma_1(\omega)$ for the whole energy range derived from the model is shown in Fig. 2(c). The inset of Fig. 2(c) shows the onset of absorption in $\sigma_1(\omega)$ which coincides with a sudden drop of transmission at 0.52 eV, 0.77 eV, and 1.23 eV for Sb, As, and P, respectively. The sharp onset of absorption due to interband transition indicates a direct band gap [21]. From the model, we can get the real part of the dielectric function, ϵ_1 (see 5 (b)). The flat part in ϵ_1 above the upper E_u phonon mode gives us the correct ϵ_e of the three compounds: $\epsilon_{e,Sb} = 17.2$, $\epsilon_{e,As} = 11.8$, and $\epsilon_{e,P} = 12.4$. Note that to get ϵ_e of $EuCd_2Sb_2$, the Drude contribution had to be removed first. Another important property we can obtain is the value of static dielectric function $\epsilon_{LST}(0)$ from the Lyddane-Sachs-Teller relation:

$$\epsilon_{LST}(0) = \epsilon_e \times \left(\frac{\omega_{LO}^2}{\omega_{TO}^2}\right) \tag{2}$$

The static dielectric constant is weakly affected by lower energy phonon modes, so we include only the higher energy phonons in its calculation. This gives $\epsilon_{LST,As}(0) = 18$, and $\epsilon_{LST,P}(0) = 18.9$.

Applying a magnetic field significantly influences the electronic band structure of $EuCd_2X_2$. False color plots in Fig. 3 illustrate these three compounds' relative magneto-transmission across a broad energy and magnetic field range. The energy gap of $EuCd_2P_2$ in Fig. 3(a) undergoes remarkable tuning at a very low magnetic field. At 0 T, the energy gap is approximately 1.23 eV, consistent with the zero-field optics shown in Fig. 2(a-b). As a magnetic field is applied, the energy gap decreases significantly, reaching 1.08 eV around 0.8 T (ΔE_g = 150 meV). Beyond 2 T, the reduction of the band gap saturates. Similar behavior is observed in the relative

Compound	T_N **(K)**	ω_{TO} **(cm^{-1})**	ω_{LO} **(cm^{-1})**	$\mathbf{E}_a$ **(meV)**	$\mathbf{E}_g$ **(eV)**	$\mathbf{J}_{\text{eff}}$ **(meV)**	**Volume of primitive cell (Å^3)**
$EuCd_2Sb_2$	7.3	138	-	-	0.52	16	148.4
$EuCd_2As_2$	9.5	165	204	26	0.77	82	125.0
$EuCd_2P_2$	11	241	298	16	1.23	92	114.4

Table I. The parameters of $EuCd_2X_2$ (X = Sb, As, P), where T_N indicates Néel temperature, ω_{TO} and ω_{LO} indicate the position of phonon TO and LO modes, respectively, E_a represents the activation energy, E_g represents the energy gap, and J_{eff} is the exchange interaction.

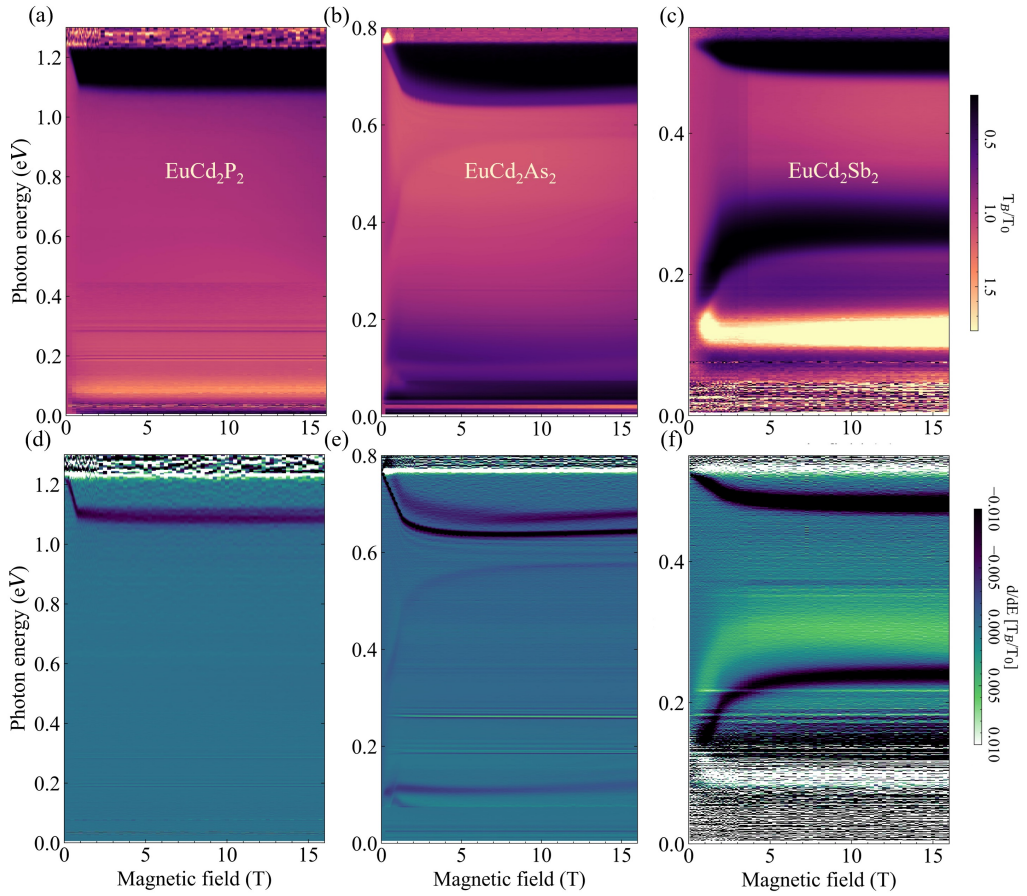


Figure 3. Relative magneto-transmission, T_B/T_0, and the derivative of the relative magneto-transmission $d/dE[T_B/T_0]$ measured at 4.2 K and shown as a function of photon energy and magnetic field for (a-d) $EuCd_2P_2$, (b-e) $EuCd_2As_2$, and (c-f) $EuCd_2Sb_2$.

magneto transmission of $EuCd_2As_2$ as reported in [1]. The gap decreases by 130 meV around a field of 1.7 T and reaches a plateau after 5 T. The energy gap in $EuCd_2Sb_2$ decreases by 45 meV around a field of 2 T then after 4 T it stays constant. The influence of the magnetic field is also clearly visible in the derivative of the magneto transmission in Fig. 3 (d-f). *Ab initio* calculations performed by Cuono et al. confirmed the energy gap of $EuCd_2As_2$ and its evolution in a magnetic field, they based their analysis on the experimental results by Cottin et al. Additionally, they extended these calculations to $EuCd_2Sb_2$ and $EuCd_2P_2$, obtaining energy gaps that closely match our experimental findings [5].

Despite its substantial reduction in the magnetic field, the band gap never closes in any of the three compounds, and no band inversion is observed. Instead, the strong redshift of the band gap, $\Delta E_g(B)$, shown in Fig. 4(b), seems to be proportional to the magnetization shown in Fig. 4(a), denoted as $M(\mu_0 H)$. This proportionality is observed in europium monochalcogenide materials such as EuTe [22], where there is a connection between the redshift of the absorption edge and the magnetization.

The observation of a connection between $\Delta E_g(B)$ and $M(\mu_0 H)$ in our systems validates the molecular field approximation, where ΔE_g can be expressed as:

$$\Delta E_g = -\frac{1}{2} J_{\text{eff}} \frac{SM(T,H)}{M_S} \tag{3}$$

Here, J_{eff} represents the effective exchange energy between band carriers and Eu spins, $S = 7/2$, and M_S is the saturation magnetization. Owing to weak overlap of the $4f$ states with other bands, we expect a minimal hybridization between the Eu bands and bands from other elements. This is why J_{eff} represents an intra-atomic exchange interaction. Applying this formula to our data, we obtain $J_{\text{eff}} = 92$ meV, 82 meV, and 16 meV for $EuCd_2X_2$ (X = P, As, and Sb) respectively. This observed exchange interaction could be attributed to an $f - d$ exchange interaction, as discussed in Ref. 22. The significant change in J_{eff} from P to Sb indicates that this interaction is notably influenced by the neighboring atoms around Eu. A potential explanation for the decreased J_{eff} when moving from P to Sb lies in the binding energies of Eu $4f$ states in these compounds or, in other terms, the position of these $4f$ states with respect to the valence band maximum. Specifically, the $4f$ state in P lies at ~ 1 eV below the valence band maximum (Fig. 1(d)), whereas for As it centered around 1.3 eV below the valence band maximum [1]. While ARPES on $EuCd_2Sb_2$ has not been reported yet, the *ab initio* calculations suggest that the $4f$ states lie even deeper than those of As and P [23]. Consequently, the $4f$ states in $EuCd_2P_2$ align more closely with the d states in the conduction band than those in $EuCd_2As_2$ and $EuCd_2Sb_2$, resulting in the observed larger J_{eff}.

The energy gap decreases from phosphorus (P) to antimony (Sb) due to the energy difference between bonding and anti-bonding orbitals, influenced by the overlap of interatomic orbitals. This overlap is affected by the atoms' electronegativity, which increases from Sb to P, as it rises to the right and upwards in the periodic table. Higher electronegativity corresponds to higher bonding energy. In $EuCd_2P_2$, there is a stronger overlap of orbitals compared to $EuCd_2As_2$. This stronger overlap leads to a greater energy splitting between bonding and anti-bonding states, indicating higher stability and a higher energy gap for the phosphide compound.

In conclusion, our study investigates the impact of substituting Sb, As, and P on the electrical and optical properties of the material. Replacing nonmetal elements like P with metalloids such as As and Sb induces changes in the band structures, consequently altering the energy gap. Importantly, this substitution does not lead to the closure of the energy gap, and the material retains its magnetic semiconducting nature. The observed redshift in the energy gap demonstrates a direct correlation with magnetization. This finding supports the application of the molecular field approximation, revealing that the magnetic properties of Eu significantly influence the band structure of this material family. Therefore, the magnetic ordering of Eu ions has a direct impact on the band structure of $EuCd_2X_2$ (X = Sb, As, P).

I. ACKNOWLEDGMENTS

This research was supported by the NCCR MARVEL, a National Centre of Competence in Research, funded by the Swiss National Science Foundation (Grant No. 205602). A. A. acknowledges funding from the Swiss National Science Foundation through project No. PP00P2_202661. N.B. acknowledges the support of the Croatian Science Foundation under Project No. IP-2022-10-3382. M. N. and N. B. acknowledge the support of the CeNIKS project co-financed by the Croatian Government and the EU through the European Regional Development Fund Competitiveness and Cohesion Operational Program (Grant No. KK.01.1.1.02.0013). We acknowledge the support of LNCMI-CNRS, a member of the European Magnetic Field Laboratory (EMFL). The work at the TU Wien was supported by FWF Project P 35945-N. Work at Brookhaven National Laboratory was supported by the Office of Science, U.S. Department of Energy under Contract No. DE-SC0012704.

II. APPENDIX

Figure 5(a) shows the reflectance of $EuCd_2X_2$ (X = Sb, As, P) over the entire energy range. The low energy extrapolation of the data, below 20 cm^{-1}, is based on an assumption that the reflectance is constant in that regime. The high energy data, above 54000 cm^{-1}, is extrapolated using X-ray scattering functions developed by Henke and coworkers [24].

The real part of the dielectric function is plotted in Figure 5(b), where it shows the flat part of ϵ_1 for energies above the second phonon. This dielectric constant was obtained from modeling the reflectivity and transmission.

Figure 6 shows how the activation energy was determined for samples of (a) $EuCd_2As_2$ and (b-c) $EuCd_2P_2$. We used the Arrhenius equation, $R = R_0 \exp\left(\frac{E_a}{k_B T}\right)$, where k_B is the Boltzmann constant, E_a is the activation energy, and T is the temperature. Samples in Fig. 6(b) and (c) have different carrier concentrations, resulting in very different activation energies. This is probably caused by slighlty different synthesis conditions.

The X-ray diffraction (XRD) analysis of $EuCd_2X_2$ (X = Sb, As, P) (Fig. 7) was performed on powders obtained by crushing single crystals. All three compounds exhibit similar peak patterns, with peaks shifting to higher angles as the lattice size decreases. Peak assignments, identified using Miller indices, were made using the PowderX software package and Crystallographic Information Files (.cif) available for these compounds.

In the case of $EuCd_2P_2$, a small impurity phase (*)

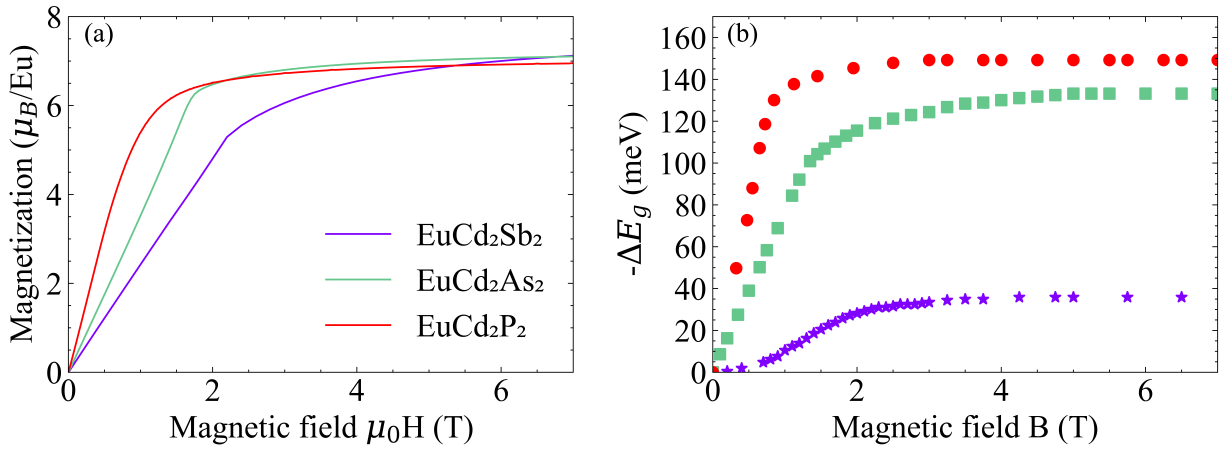


Figure 4. (a) The magnetization as a function of the magnetic field at 4 K for $EuCd_2X_2$ (X = Sb, As, P) with a saturation of around $M_{sat} = 7\ \mu_B$. (b) The onset of absorption extracted from the magneto transmission color plots, for $EuCd_2X_2$ (X = Sb, As, P) exhibits a behavior similar to that of the magnetization.

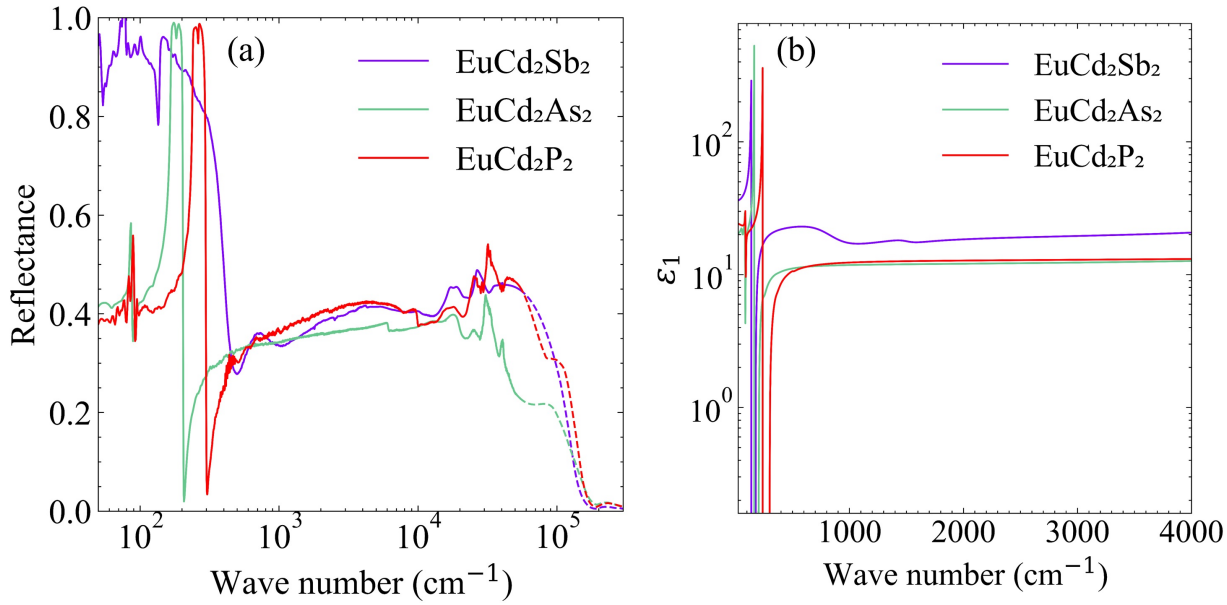


Figure 5. (a) The full range energy reflectance of $EuCd_2X_2$ (X = Sb, As, P) at 10 K. (b) The low-energy real part of the dielectric constant ϵ_1 of $EuCd_2X_2$ (X = Sb, As, P) at 10 K extracted from the model.

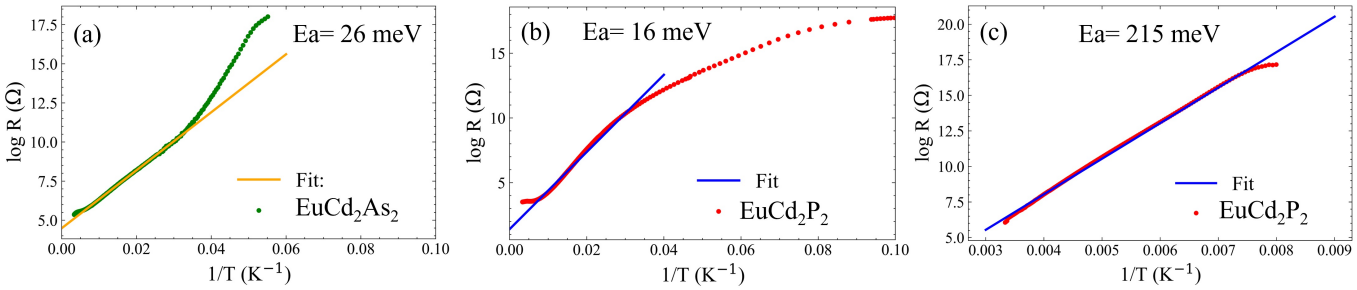


Figure 6. (a) Activation energy extraction by fitting the resistance of $EuCd_2As_2$. (b-c) $EuCd_2P_2$.

was detected, likely originating from a secondary flux phase located on the crystal surface or at crystal bound-

aries. Crystallization of $EuCd_2P_2$ predominantly yielded smaller crystals, and multiple crystals had to be selected and crushed for the XRD measurement, potentially introducing this unwanted phase into the XRD pattern.

[1] D. Santos-Cottin, I. Mohelský, J. Wyzula, F. Le Mardelé, I. Kapon, S. Nasrallah, N. Barišić, I. Živković, J. R. Soh, F. Guo, K. Rigaux, M. Puppin, J. H. Dil, B. Gudac, Z. Rukelj, M. Novak, A. B. Kuzmenko, C. C. Homes, T. Dietl, M. Orlita, and A. Akrap, $EuCd_2As_2$: A magnetic semiconductor, Physical Review Letters **131**, 186704 (2023).

[2] R. A. Nelson, J. King, S. Cheng, A. J. Williams, C. Jozwiak, A. Bostwick, E. Rotenberg, S. Sasmal, I.-H. Kao, A. Tiwari, N. R. Jones, C. Cai, E. Martin, A. Dolocan, L. Shi, R. K. Kawakami, J. P. Heremans, J. Katoch, and J. E. Goldberger, Revealing the EuCd2As2 semiconducting band gap via n-type la-doping, Chemistry of Materials 10.1021/acs.chemmater.4c00656 (2024).

[3] S. Nishihaya, A. Nakamura, M. Ohno, M. Kriener, Y. Watanabe, M. Kawasaki, and M. Uchida, Intrinsic insulating transport characteristics in low-carrier density EuCd2As2 films, Applied Physics Letters **124**, 023103 (2024).

[4] Y. Shi, Z. Liu, L. A. Burnett, S. Lee, C. Hu, Q. Jiang, J. Cai, X. Xu, M. Li, C.-C. Chen, and J.-H. Chu, Absence of weyl nodes in EuCd2As2 revealed by the carrier density dependence of the anomalous hall effect, Phys. Rev. B **109**, 125202 (2024).

[5] G. Cuono, R. M. Sattigeri, C. Autieri, and T. Dietl, Ab initio overestimation of the topological region in Eu-based compounds, Phys. Rev. B **108**, 075150 (2023).

[6] G. Hua, S. Nie, Z. Song, R. Yu, G. Xu, and K. Yao, Dirac semimetal in type-iv magnetic space groups, Phys. Rev. B **98**, 201116(R) (2018).

[7] L.-L. Wang, N. H. Jo, B. Kuthanazhi, Y. Wu, R. J. McQueeney, A. Kaminski, and P. C. Canfield, Single pair of weyl fermions in the half-metallic semimetal $EuCd_2As_2$, Phys. Rev. B **99**, 245147 (2019).

[8] H. Su, B. Gong, W. Shi, H. Yang, H. Wang, W. Xia, Z. Yu, P.-J. Guo, J. Wang, L. Ding, L. Xu, X. Li, X. Wang, Z. Zou, N. Yu, Z. Zhu, Y. Chen, Z. Liu, K. Liu, G. Li, and Y. Guo, Magnetic exchange induced Weyl state in a semimetal EuCd2Sb2, APL Materials **8**, 011109 (2020).

[9] J. Ma, H. Wang, S. Nie, C. Yi, Y. Xu, H. Li, J. Jandke, W. Wulfhekel, Y. Huang, D. West, P. Richard, A. Chikina, V. N. Strocov, J. Mesot, H. Weng, S. Zhang, Y. Shi, T. Qian, M. Shi, and H. Ding, Emergence of nontrivial low-energy dirac fermions in antiferromagnetic EuCd2As2, Advanced Materials **32**, 1907565 (2020).

[10] Y. Goryunov, V. Fritsch, H. v. Löhneysen, and A. Nateprov, The esr study of eu ternary pnictides EuCd2Sb2, EuZn2As2, Journal of Physics: Conference Series **391**, 012015 (2012).

[11] I. Schellenberg, U. Pfannenschmidt, M. Eul, C. Schwickert, and R. Pöttgen, A 121Sband 151Eu mössbauer spectroscopic investigation of EuCd2X2 (X = P, As, Sb) and YbCd2Sb2, Zeitschrift für anorganische und allgemeine Chemie **637**, 1863 (2011).

[12] V. Sunko, Y. Sun, M. Vranas, C. C. Homes, C. Lee, E. Donoway, Z.-C. Wang, S. Balguri, M. B. Mahendru, A. Ruiz, B. Gunn, R. Basak, S. Blanco-Canosa, E. Schierle, E. Weschke, F. Tafti, A. Frano, and J. Orenstein, Spin-carrier coupling induced ferromagnetism and giant resistivity peak in $EuCd_2P_2$, Phys. Rev. B **107**, 144404 (2023).

[13] H. Zhang, L. Fang, M.-B. Tang, H.-H. Chen, X.-X. Yang, X. Guo, J.-T. Zhao, and Y. Grin, Synthesis and properties of CaCd2Sb2 and EuCd2Sb2, Intermetallics **18**, 193 (2010).

[14] Y. Shi, Z. Liu, L. A. Burnett, S. Lee, C. Hu, Q. Jiang, J. Cai, X. Xu, M. Li, C.-C. Chen, and J.-H. Chu, Absence of weyl nodes in $EuCd_2As_2$ revealed by the carrier density dependence of the anomalous hall effect, Phys. Rev. B **109**, 125202 (2024).

[15] J.-R. Soh, E. Schierle, D. Y. Yan, H. Su, D. Prabhakaran, E. Weschke, Y. F. Guo, Y. G. Shi, and A. T. Boothroyd, Resonant x-ray scattering study of diffuse magnetic scattering from the topological semimetals $EuCd_2As_2$ and $EuCd_2Sb_2$, Phys. Rev. B **102**, 014408 (2020).

[16] D. Y. Usachov, S. Krebber, K. A. Bokai, A. V. Tarasov, M. Kopp, C. Garg, A. Virovets, J. Müller, M. Mende, G. Poelchen, D. V. Vyalikh, C. Krellner, and K. Kliemt, Magnetism, heat capacity, and electronic structure of $EuCd_2P_2$ in view of its colossal magnetoresistance, Phys. Rev. B **109**, 104421 (2024).

[17] C. C. Homes, Z.-C. Wang, K. Fruhling, and F. Tafti, Optical properties and carrier localization in the layered phosphide $EuCd_2P_2$, Phys. Rev. B **107**, 045106 (2023).

[18] D. B. Tanner, *Optical Effects in Solids* (Cambridge University Press, Cambridge, 2019).

[19] A. Gourgout, M. Leroux, J.-L. Smirr, M. Massoudzadegan, R. P. S. M. Lobo, D. Vignolles, C. Proust, H. Berger, Q. Li, G. Gu, C. C. Homes, A. Akrap, and B. Fauqué, Magnetic freeze-out and anomalous hall effect in ZrTe5, npj Quantum Materials **7**, 71 (2022).

[20] A. B. Kuzmenko, KramersKronig constrained variational analysis of optical spectra, Review of Scientific Instruments **76**, 083108 (2005).

[21] P. Y. Yu and M. Cardona, *Fundamentals of Semiconductors* (Springer, Berlin Heidelberg, 2010).

[22] L. Schmutz, G. Dresselhaus, and M. Dresselhaus, Optical absorption of EuTe in high magnetic fields, Solid State Communications **28**, 597 (1978).

[23] H. Su, B. Gong, W. Shi, H. Yang, H. Wang, W. Xia, Z. Yu, P.-J. Guo, J. Wang, L. Ding, L. Xu, X. Li, X. Wang, Z. Zou, N. Yu, Z. Zhu, Y. Chen, Z. Liu, K. Liu, G. Li, and Y. Guo, Magnetic exchange induced Weyl state in a semimetal EuCd2Sb2, APL Materials **8**, 011109 (2020).

[24] B. Henke, E. Gullikson, and J. Davis, X-ray interactions: Photoabsorption, scattering, transmission, and reflection at E = 50-30,000 eV, Z = 1-92, Atomic Data and Nuclear Data Tables **54**, 181 (1993).

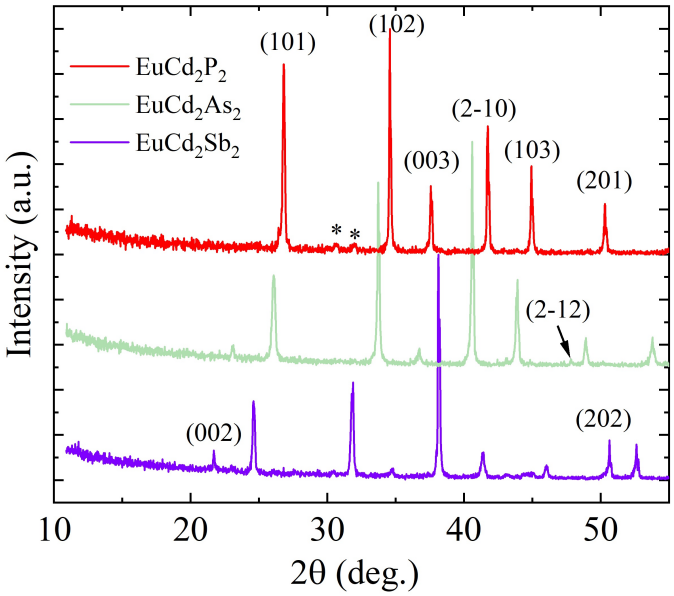


Figure 7. Powder XRD for $EuCd_2X_2$ (X=Sb, As, P) obtained from crushed single crystals. All three compounds are isovalent and crystallize in trigonal crystal structure with space group P-3m1 (164). Prominent peaks are marked by Miller indices. Two small peaks (*) in $EuCd_2P_2$ may come from the remaining flux or an impurity phase formed at the crystal boundaries.